Materials and Design 31 (2010) 296–305

Contents lists available at ScienceDirect

Materials and Design

journal homepage: www.elsevier.com/locate/matdes

Influence of continuum damage mechanics on the Bree's diagram of a closed end tube

A. Nayebi *

Department of Mechanical Engineering, Shiraz University, Shiraz, Iran

ARTICLE INFO

Article history:
Received 30 April 2009
Accepted 11 June 2009
Available online 13 June 2009

Keywords:
Continuum damage mechanics
Nonlinear kinematic hardening
Bree's diagram
Shakedown
Ratcheting
Return mapping algorithm

ABSTRACT

This paper extends the Bree's cylinder behaviors, which is subjected to the constant internal pressure and cyclic temperature gradient loadings, with considering continuum damage mechanics coupled with nonlinear kinematic hardening model. The Bree's biaxial stress model is modified using the unified damage and the Armstrong–Frederick nonlinear kinematic hardening models. With the help of the return mapping algorithm, the incremental plastic strain in axial and tangential directions is obtained. Continuum damage mechanics approach can be used to extend the Bree's diagram to the damaging structures and reduce the plastic shakedown domain. Kinematic hardening behavior was considered in the material model which shifts the ratcheting zone. The role of the material constants in the Bree's diagram is also discussed.

1. Introduction

The need for a suitable constitutive model to predict the shakedown or cyclic failure (ratcheting) of structures under cyclic loading is increasing in many industries, and in order to better obtain the structures behaviors, many researchers tried to develop improved constitutive models [1]. Although, the proposed models simulate well the uniaxial ratcheting responses, there are other factors that influence the biaxial stress cyclic loading. Shakedown loads and different behaviors of structures were also studied by many authors with the plasticity and cyclic plasticity models [2]. In particular, the two-bar problem and the Bree's cylinder were studied under different loading conditions and materials behaviors. Parkes [3] studied thermal ratcheting in an aircraft wing resulting from the cyclic thermal stresses superimposed on the normal wing loads. Miller [4] showed that the material strain hardening reduces considerably the strains due to ratcheting in the two-bar structure. Jiang and Leckie [5] presented a method for direct determination of the steady solutions in shakedown analysis with application to the two-bar problem. Bree [6] analyzed the elastic–plastic behavior of a thin cylindrical tube subjected to constant internal pressure and cyclic temperature gradient across the tube thickness. A simple one-dimensional model, a linear temperature drop distribution across the cylinder thickness and an elastic–perfectly-plastic material model were assumed in his analysis. Later, he used a biaxial stress model and obtained a more complete interaction diagram (Bree's diagram) for a closed tube [7]. In that study the material was assumed to be perfect plastic. The Poisson's effect was also neglected. The interaction diagram proposed by Bree received adequate investigation by a number of researchers [8,9]. His one-dimensional diagram is a part of ASME boiler and pressure vessel code [8] (Fig. 1). Mulcahy [9] improved the Bree's analysis with incorporating a linear kinematic hardening model in the analysis of a beam element.

Classical shakedown theory of Melan–Koiter for elastic–perfectly-plastic bodies has been well established in the literature [10]. Melan procedure for the shakedown theorem can also be extended to encompass the linear kinematic hardening, but one encounters mathematical difficulty in treating more general cases, and the procedure does not apply straightforwardly for the case of Prager's linear kinematic hardening. It seems that some additional assumptions as well as further mathematical tricks are needed to deal with the general kinematic hardening. Recently, Abdalla et al. [11] proposed a simple shakedown method with perfect plasticity material behavior to study the Bree's cylinder problem and the 90° pipes bending.

Very limited work has been done on damage related to the interaction diagram. The shakedown theory has been extended to include hardening and damage by Hachemi and Weichert [12] and Druyanov and Roman [13]. However, the extensions should be made often at the expense of losing certain fine features of the classical plasticity theory and shakedown theorems. Without the theorems in Melan–Koiter sense, which are valid only with certain restrictions, generally in practice one has to implement numerical incremental analysis to check for shakedown of a

* Tel.: +98 711 6133029.
E-mail address: nayebi@shirazu.ac.ir

0261-3069/$ - see front matter © 2009 Elsevier Ltd. All rights reserved.
doi:10.1016/j.matdes.2009.06.014

Nomenclature

A	virgin surface
$\tilde{A}$	resistant effective surface
C	NLKH model's constant
D_c	interatomic decohesion damage parameter
E	elastic modulus
$\tilde{E}$	effective elastic modulus
e_z	nondimensional axial strain
e_θ	nondimensional tangential strain
f	yield function
F_ϖ	dissipative potential function
K_1	mean tangential strain
K_2	mean axial strain
n_{ij}	outward normal to the yield surface
P	internal pressure
$\dot{p}$	equivalent plastic strain rate
Δp	equivalent plastic strain increment
q	material damage constant
Q	material damage constant
r	mean radius
R_υ	triaxiality function
S_z	nondimensional axial stress
S_θ	nondimensional tangential stress
t	thin wall thickness
T	temperature
ΔT	temperature difference between the inner and outer surfaces
ΔT_x	temperature difference in each radius
x	coordinate
$\boldsymbol{X}$	back stress tensor
$\boldsymbol{X'}$	deviatoric back stress tensor
Y	associate thermodynamics damage variable tensor
α	expansion coefficient
γ	NLKH model's constant
$d\lambda$	incremental plastic multiplier
η	nondimensional thickness
$\boldsymbol{\varepsilon^p}$	plastic strain tensor
$\boldsymbol{\varepsilon^T}$	thermal strain tensor
ε_D^p	plastic damage threshold strain
$\boldsymbol{\sigma}$	stress tensor
$\tilde{\boldsymbol{\sigma}}$	effective stress tensor
$\boldsymbol{\sigma'}$	deviatoric stress tensor
σ_{eq}	equivalent von-Mises stress
σ_H	hydrostatic stress
σ_P	nondimensional mechanical stress parameter
σ_y	yield stress
τ	nondimensional temperature difference
$\Delta\tau$	nondimensional temperature difference increment
υ	Poisson's ratio
ϖ	damage parameter

structure under specific loading histories. Recently, Nayebi and El Abdi [14] and Kang et al. [15] used continuum damage mechanics (CDM) to predict the material behavior, including ratcheting and shakedown in 1-D analysis.

In this research, the effect of continuum damage mechanics on the Bree's diagram of a thin cylinder structure under specific loading histories is studied. Nonlinear kinematic hardening (NLKH) theory is coupled with continuum damage mechanics in order to model the behavior of the Bree's cylinder. A unified damage mechanics model, which is also appropriate for low cyclic loading, is used. During each loading, the damage analysis is performed. An iterative method is used to analyze the cylinder under the cyclic thermal and constant mechanical loads. The model extends Bree's 2-D diagram to incorporate damage effects. The proposed method can also be applied to other structures subjected to cyclic thermal and constant mechanical loadings. The results illustrate the influence of material damage on the behaviors of structures under cyclic loading in comparison with the confirmed results on undamaged structures.

2. Constitutive behavior relations

2.1. Continuum damage mechanics

According to the applied theory of damage mechanics, microscopic change in a material element of surface A develops into macroscopic defect as a result of loading. In the damaged state, the new area is denoted by $\tilde{A}$ (Fig. 2), from which the isotropic damage variable ϖ is defined as [16]

$$\varpi = \frac{A - \tilde{A}}{A}, \tag{1}$$

where ϖ may be considered as an internal state variable characterizing the irreversible deterioration of a material in the thermodynamic sense. Following this theory, the behavior of a damaged material can then be represented by the constitutive equations of the virgin material where the usual stress tensor, σ, is replaced by the effective stress $\tilde{\boldsymbol{\sigma}}$ defined by

$$\tilde{\boldsymbol{\sigma}} = \frac{\boldsymbol{\sigma}}{1 - \varpi}, \tag{2}$$

where the value $\varpi = 0$ corresponds to the undamaged state, $\varpi \in (0, D_c)$ corresponds to a partly damaged state, and $\varpi = D_c$ defines the element state rupture by interatomic decohesion ($D_c \in [0, 1]$). In the sequel, superposed tilde indicates quantities related to the damaged state of the material.

From a physical point of view, the material degradation involves the initiation, growth and coalescence of micro-cracks or microvoids generally induced by large plastic strains. This phenomenon is called ductile plastic damage and leads to plastic (ductile) fracture. Many observations and experiments indicated that the damage is also governed by the plastic strain which is introduced into the model through the plastic multiplier $\dot{\lambda}$, as [16]

$$\dot{\varpi} = \dot{\lambda}\frac{\partial F_\varpi}{\partial Y} \quad \text{if } \varepsilon^p \succ \varepsilon_D^p, \tag{3}$$

where $\dot{\lambda}$ is calculated from the constitutive equations of plasticity coupled with the damage deduced from the dissipative potential function, F_ϖ. Y is the associate variable of the damage rate, $\dot{\varpi}$, and ε_D^p is the plastic damage threshold strain. Also, many experimental results indicated that F_ω must be a nonlinear function of Y [16]

$$F_\varpi = \frac{Q}{(q+1)(1-\varpi)}\left(\frac{Y}{Q}\right)^{q+1} \tag{4}$$

from which Eq. (3) reduces to

$$\dot{\varpi} = \left(\frac{Y}{Q}\right)^q \dot{p} \tag{5}$$

where Q and q are material parameters and $\dot{p}$ is the equivalent plastic strain rate. According to Lemaitre and Desmorat [16]

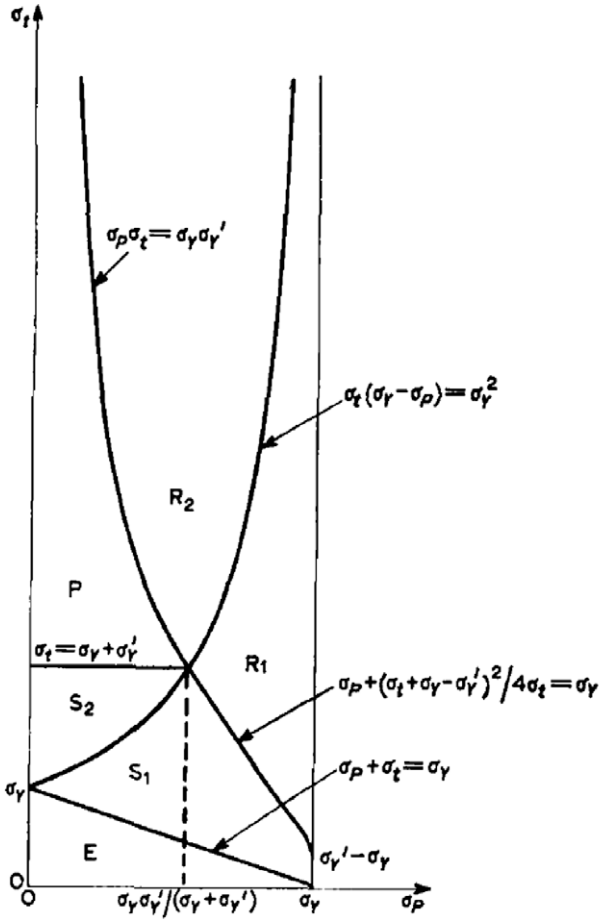

Stress regime	Thin tube behavior
R_1 and R_2	Ratcheting
S_1 and S_2	Shakedown after first half cycle
P	Plastic cycling
E	Elastic

Fig. 1. Bree's diagram for a 1-D tube model [6].

$$\begin{cases} Y = \frac{\sigma_{eq}^2 R_\upsilon}{2E} \\ R_\upsilon = \frac{2}{3}(1+\upsilon) + 3(1-2\upsilon)\left(\frac{\sigma_H}{\sigma_{eq}}\right)^2, \end{cases} \tag{6}$$

where R_υ is the triaxiality function of stress, $\sigma_{eq} = (3/2\boldsymbol{\sigma}':\boldsymbol{\sigma}')^{1/2}$ is the von-Mises equivalent stress ($\sigma_{ij}' = \sigma_{ij} - \sigma_H\delta_{ij}$ and: indicates the inner product of two tensors), $\sigma_H = 1/3\mathrm{tr}(\boldsymbol{\sigma})$ denotes the hydrostatic stress (δ_{ij} is the Kronecker unit tensor), E is Young modulus, and υ is the Poisson's ratio. Using Eqs. (2) and (6), one can reduce the damage law (Eq. (5)) to the unified damage law for low cycle fatigue as [16]

$$\dot{\varpi} = \left(\frac{\sigma_{eq}^2 R_\upsilon}{2EQ(1-\varpi)^2}\right)^q \dot{p}, \tag{7}$$

where $\dot{p}$ is the accumulated plastic strain rate given by

$$\dot{p} = \left(\frac{2}{3}\dot{\varepsilon}^p : \dot{\varepsilon}^p\right)^{\frac{1}{2}} \tag{8}$$

So, the damage parameter is related to the equivalent plastic strain and is coupled with the plasticity. Assuming the von-Mises yield criteria, the yield surface can be rewritten by replacing the stress with the effective stress $\tilde{\boldsymbol{\sigma}}$, as

$$f(\tilde{\boldsymbol{\sigma}}, \boldsymbol{X}) = f\left(\frac{\boldsymbol{\sigma}}{1-\varpi}, \boldsymbol{X}\right), \tag{9}$$

where $\boldsymbol{X}$ is the back stress.

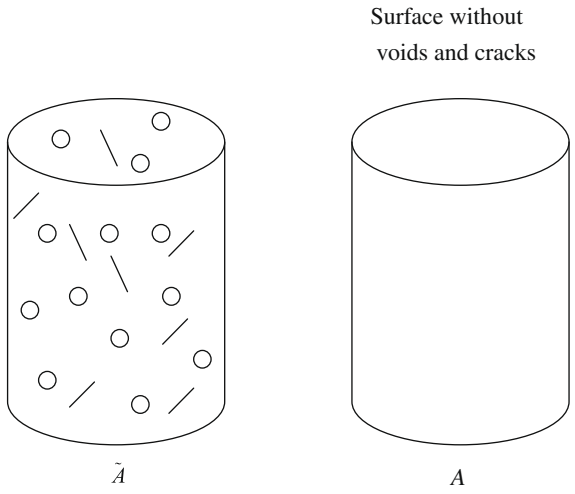

Fig. 2. Definition of the surface (A) and the effective resistant surface ($\tilde{A}$).

2.2. Nonlinear kinematic hardening

Nonlinear kinematic hardening is introduced using the differential form of the governing equations for the kinematic variables. Based on the von-Mises yield criteria, the equation of the yield surface is written as

$$f = J_2(\tilde{\boldsymbol{\sigma}} - \boldsymbol{X}) - \sigma_y = \left[\frac{3}{2}(\tilde{\boldsymbol{\sigma}}' - \boldsymbol{X}') : (\tilde{\boldsymbol{\sigma}}' - \boldsymbol{X}')\right]^{\frac{1}{2}} - \sigma_y = 0, \tag{10}$$

where X is the back stress defining the position of the yield surface and σ_y characterizes the size of the surface. The plastic flow follows the normality rule

$$d\boldsymbol{\varepsilon}^p = \frac{d\lambda}{1-\varpi}\frac{\partial f}{\partial \boldsymbol{\sigma}} = \frac{3}{2}\frac{d\lambda}{1-\varpi}\frac{(\tilde{\boldsymbol{\sigma}}' - \boldsymbol{X}')}{(\tilde{\boldsymbol{\sigma}}' - \boldsymbol{X}')_{eq}}. \tag{11}$$

The plastic multiplier $d\lambda$ is derived from the consistency condition, $f = df = 0$, if plastic flow occurs. Different kinematic hardening models are available for the plastic analysis of structures. Sehitoglu et al. [17] pointed out that the material model was critical for the stress analysis of a damaged component. Many cyclic plasticity models were tested under different cyclic loadings [18–21]. A number of loading responses may be predicted by these models, while they fail to predict other types of cyclic loading conditions. Accordingly, it is difficult to understand which case of loading should be simulated with which model. In this paper, the Armstrong–Frederick nonlinear kinematic hardening model [22] coupled with continuum damage mechanics is used to determine the structure behavior under cyclic loadings.

If the plastic strain (ε_{ij}^p) and the back stress tensor (X_{ij}) are assumed as the internal variables, the evolution equations are

(a) Flow rule:

$$d\varepsilon_{ij}^p = d\lambda n_{ij}, \tag{12}$$

where $n_{ij} = \frac{\partial f}{\partial \sigma_{ij}} = \frac{3}{2}\frac{1}{1-\varpi}\frac{\tilde{\sigma}'_{ij} - X'_{ij}}{\|\tilde{\sigma}_{ij} - X_{ij}\|}$ is the outward normal to the yield surface and $d\lambda$ is the incremental plastic multiplier calculated from the consistency condition

$$df = \frac{\partial f}{\partial \sigma_{ij}}d\sigma_{ij} + \frac{\partial f}{\partial X_{ij}}dX_{ij} + \frac{\partial f}{\partial \varpi}d\varpi = 0, \tag{13}$$

(b) Nonlinear kinematic hardening model

$$dX_{ij} = \frac{2}{3}C(1-\varpi)d\varepsilon_{ij}^p + \gamma X_{ij}d\lambda, \tag{14}$$

where C and γ are material parameters and

$$d\lambda = (1-\varpi)dp \tag{15}$$

3. Closed-tube biaxial-stress model based on CDM

The studied pressure vessel was assumed to be a thin cylinder with the mean radius r, and the wall thickness, t. It is closed at both ends. The thin cylinder is subjected to an internal pressure P and a heat flux through its internal surface (Fig. 3). The temperature difference decreases linearly across the wall thickness and is changed cyclically between ΔT and zero. It is assumed that the cylindrical shell is very long and the end effects and the curvature can be neglected.

The axial and hoop strains, ε_z and ε_θ, are spatially constant [8]. This is because of the bending prevention; however they change during each cycle. The axial and hoop stresses, σ_z and σ_θ, vary across the thickness and are only dependent on the coordinate x shown in the Fig. 3a. Using the equilibrium conditions, it is required that

$$\int_{\frac{-t}{2}}^{\frac{t}{2}} \sigma_\theta dx = Pr, \tag{16}$$

$$\int_{\frac{-t}{2}}^{\frac{t}{2}} \sigma_z dx = \frac{Pr}{2} \tag{17}$$

Consequently, every element of the tube is subjected to the mean stress $\frac{Pr}{2t}$ in axial direction and $\frac{Pr}{t}$ in hoop direction. The temperature difference in start up half cycle is assumed to vary linearly with respect to x. It is zero in the thin cylinder mid-wall and at the shutdown second half cycle

$$\Delta T_x = -\frac{x}{t}\Delta T, \tag{18}$$

where ΔT is the temperature difference between inner and outer surface of the tube. The mean temperature in each cycle was assumed sufficiently low so that creep effects could be ignored. Fig. 3 demonstrates the loading steps.

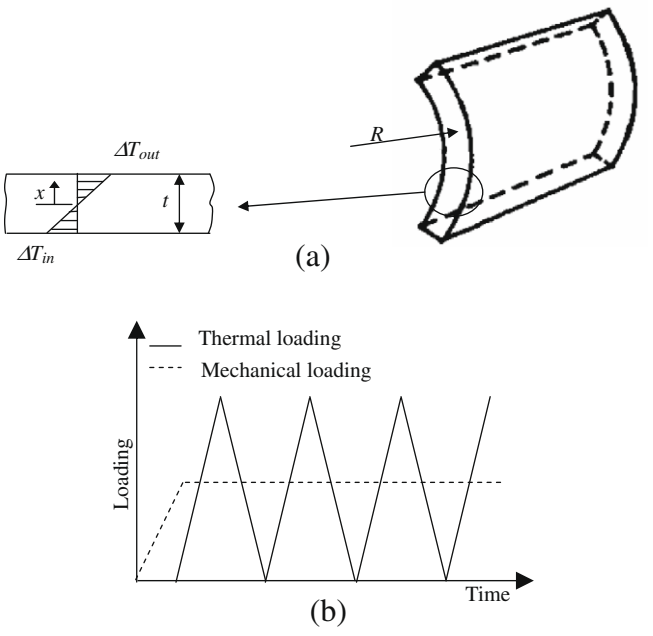

Fig. 3. (a) Tube geometry and applied temperature gradient across the tube wall thickness, t, (b) constant mechanical and cyclic temperature gradient loadings history.

Since bending is prevented in both hoop and axial direction, ε_θ and ε_z are constants across the tube thickness. Therefore, the total strain in both directions and for every loading is constant

$$\varepsilon_\theta = K_1 \tag{19}$$

$$\varepsilon_z = K_2 \tag{20}$$

Using the strain partition principle, the strains in hoop and axial direction have three parts (in small strain hypothesis): elastic, thermal and plastic strains. The total strains in two directions are:

$$\varepsilon_\theta = \varepsilon_\theta^e + \varepsilon_\theta^T + \varepsilon_\theta^p = \left(\frac{\tilde{\sigma}_\theta}{E} - \upsilon\frac{\tilde{\sigma}_z}{E}\right) + \alpha\Delta T_x + \varepsilon_\theta^p \tag{21}$$

$$\varepsilon_z = \varepsilon_z^e + \varepsilon_z^T + \varepsilon_z^p = \left(\frac{\tilde{\sigma}_z}{E} - \upsilon\frac{\tilde{\sigma}_\theta}{E}\right) + \alpha\Delta T_x + \varepsilon_z^p \tag{22}$$

where ε^e, ε^T and ε^p are elastic, thermal and plastic strains, respectively. $\tilde{\sigma}_\theta$ and $\tilde{\sigma}_z$ are effective tangential and longitudinal stresses according to the continuum damage mechanics. They are defined in the Section 2.1. Eqs. (18)–(22) were solved to obtain hoop and axial stresses as

$$\tilde{\sigma}_\theta = \frac{E}{1-\upsilon^2}(K_1 + \upsilon K_2 - (1+\upsilon)\alpha\Delta T_x - \varepsilon_\theta^p - \upsilon\varepsilon_z^p), \tag{23}$$

$$\tilde{\sigma}_z = \frac{E}{1-\upsilon^2}(K_2 + \upsilon K_1 - (1+\upsilon)\alpha\Delta T_x - \varepsilon_z^p - \upsilon\varepsilon_\theta^p) \tag{24}$$

Substituting Eqs. (19) and (20) into Eqs. (21) and (22) and using Eqs. (16) and (17), we can determine the constants K_1 and K_2 as

$$K_1 = \frac{\left(1-\frac{\upsilon}{2}\right)\frac{Pr}{E} + \int_{-\frac{t}{2}}^{\frac{t}{2}}(1-\varpi)(\alpha\Delta T_x + \varepsilon_\theta^p)dx}{\int_{-\frac{t}{2}}^{\frac{t}{2}}(1-\varpi)dx}, \tag{25}$$

$$K_2 = \frac{\left(\frac{1}{2}-\upsilon\right)\frac{Pr}{E} + \int_{-\frac{t}{2}}^{\frac{t}{2}}(1-\varpi)(\alpha\Delta T_x + \varepsilon_z^p)dx}{\int_{-\frac{t}{2}}^{\frac{t}{2}}(1-\varpi)dx}. \tag{26}$$

In this part the following dimensionless parameters are presented:

$$\begin{cases} e_\theta^p = \frac{\varepsilon_\theta^p}{\varepsilon_y}, \quad e_z^p = \frac{\varepsilon_z^p}{\varepsilon_y}, \quad \eta = \frac{x}{t}, \\ S_\theta = \frac{\sigma_\theta}{\sigma_y}, \quad S_z = \frac{\sigma_z}{\sigma_y}, \quad \sigma_p = \frac{Pr}{tE\varepsilon_y} \\ k_1 = \frac{K_1}{\varepsilon_y}, \quad k_2 = \frac{K_2}{\varepsilon_y}, \quad \varepsilon_y = \frac{\sigma_y}{E} \end{cases} \tag{27}$$

Using these dimensionless parameters, we can simplify Eqs. (25) and (26).

$$k_1 = \frac{\left(1-\frac{\upsilon}{2}\right)\sigma_p + \int_{-\frac{1}{2}}^{\frac{1}{2}}(1-\varpi)(\alpha\Delta T_x/\varepsilon_y + e_\theta^p)d\eta}{\int_{-\frac{1}{2}}^{\frac{1}{2}}(1-\varpi)d\eta} \tag{28}$$

$$k_2 = \frac{\left(\frac{1}{2}-\upsilon\right)\sigma_p + \int_{-\frac{1}{2}}^{\frac{1}{2}}(1-\varpi)(\alpha\Delta T_x/\varepsilon_y + e_z^p)d\eta}{\int_{-\frac{1}{2}}^{\frac{1}{2}}(1-\varpi)d\eta} \tag{29}$$

Substituting the above relations for k_1 and k_2 into Eqs. (23) and (24), we can obtain the nondimensional stresses as a function of plastic strains as

$$S_\theta = (1-\varpi)\left(\frac{\sigma_p + \frac{1}{(1-\upsilon^2)}\left[\int_{-\frac{1}{2}}^{\frac{1}{2}}(1-\varpi)(e_\theta^p + \upsilon e_z^p + \tau)d\eta\right]}{\int_{-\frac{1}{2}}^{\frac{1}{2}}(1-\varpi)d\eta} - \frac{1}{(1-\upsilon^2)}(e_\theta^p + \upsilon e_z^p) - \tau\right) \tag{30}$$

$$S_z = (1-\varpi)\left(\frac{\frac{1}{2}\sigma_p + \frac{1}{(1-\upsilon^2)}\left[\int_{-\frac{1}{2}}^{\frac{1}{2}}(1-\varpi)(e_z^p + \upsilon e_\theta^p + \tau)d\eta\right]}{\int_{-\frac{1}{2}}^{\frac{1}{2}}(1-\varpi)d\eta} - \frac{1}{(1-\upsilon^2)}(e_z^p + \upsilon e_\theta^p) - \tau\right) \tag{31}$$

Table 1
Materials models constants [16].

E	υ	σ_y	γ	C	Q	q	ε_D^p	D_c
134 GPa	0.3	85 MPa	250	5500 MPa	0.6 MPa	2	0.2 ε_y	0.2

where

$$\begin{cases} \sigma_p = \frac{Pr}{t\sigma_y} \\ \tau = \frac{\alpha\Delta T_x}{\varepsilon_y(1-\upsilon)} \end{cases} \tag{32}$$

Plastic strains can be determined from the constitutive relations that include the yield criterion, the normality rule, and the back stress model. The yield function for the biaxial stress using von-Mises criterion is

$$f = (\tilde{\sigma}_\theta - X_\theta)^2 + (\tilde{\sigma}_z - X_z)^2 - (\tilde{\sigma}_\theta - X_\theta)(\tilde{\sigma}_z - X_z) - \sigma_y^2 = 0 \tag{33}$$

By the normality rule, Eq. (11), the relation between hoop and axial plastic strain increments can be obtained as

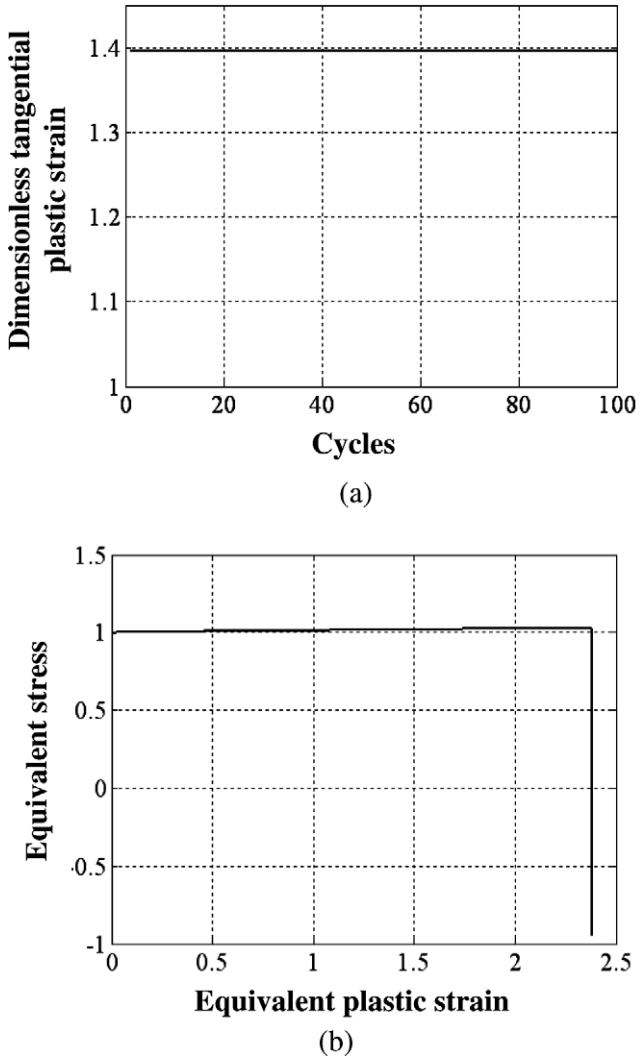

Fig. 4. Elastic shakedown behavior of the thin cylinder for τ_{max} = 1.976 and σ_p = 0.5, material models constants are given in Table 1. (a) variation of the maximum nondimensional tangential plastic strain, e_θ^p, at the outer surface of the thin cylinder as a function of the number of thermal loading cycles and (b) normalized equivalent stress versus normalized equivalent plastic strain at the outer surface.

$$\frac{d\varepsilon_z^p}{d\varepsilon_\theta^p} = \frac{2\tilde{\sigma}_z - \tilde{\sigma}_\theta - 2X_z + X_\theta}{2\tilde{\sigma}_\theta - \tilde{\sigma}_z - 2X_\theta + X_z} \tag{34}$$

In order to obtain the variations of the plastic strain and stresses, Eqs. (7), (14), (30), (31), (33), and (34) are to be solved.

4. Numerical procedure

In order to solve Eqs. (30), (31), (33), and (34), the return mapping algorithm RMA [23,24] was used. This method represents a well established integration scheme to integrate the rate constitutive equations. This method consists of an elastic trial and plastic corrector step. When the yield function is convex, i.e. $f_n^{trial} > f_n$ at time step n, the elastic trial step is employed to characterize the plastic loading/unloading state of the material using the algorithmic Kuhn–Tucker conditions

$$f_n \le 0, \quad \Delta\lambda_n \le 0, \quad \Delta\lambda_n f_n = 0. \tag{35}$$

where $\Delta\lambda_n$ is the increment of the plastic multiplier.

At each time step, the yield function is evaluated at the trial elastic step, in order to determine whether the yield occurs or not. If the trial yield function is less than zero, then the material is assumed to be elastic or plastic but under elastic unloading. Otherwise, the material is subjected to the plastic loading. The normality rule is used to define the plastic strain increment in the radial RMA. The yield condition is used to determine the incremental value of the plastic multiplier $\Delta\gamma_n$ at the current time step n. Since a nonlinear kinematic hardening is assumed, an iterative procedure is required to determine the plastic strain at the current time step. Having determined $\Delta\gamma_n$, one can update the plastic strains and the hardening parameter, and the stress at the current time step is calculated using updated parameters.

The increment of plastic damage parameter, $\Delta\varpi_{n+1}$, is updated with the help of plastic increment computations. Total damage parameter can be obtained as: $\varpi_n + \Delta\varpi_{n+1} = \varpi Z_{n+1}$. The new value of the damage parameter is used to obtain the studied parameters for the new increment of loading. In order to obtain the trial elastic solution of the model, Eqs. (30) and (31) were modified to

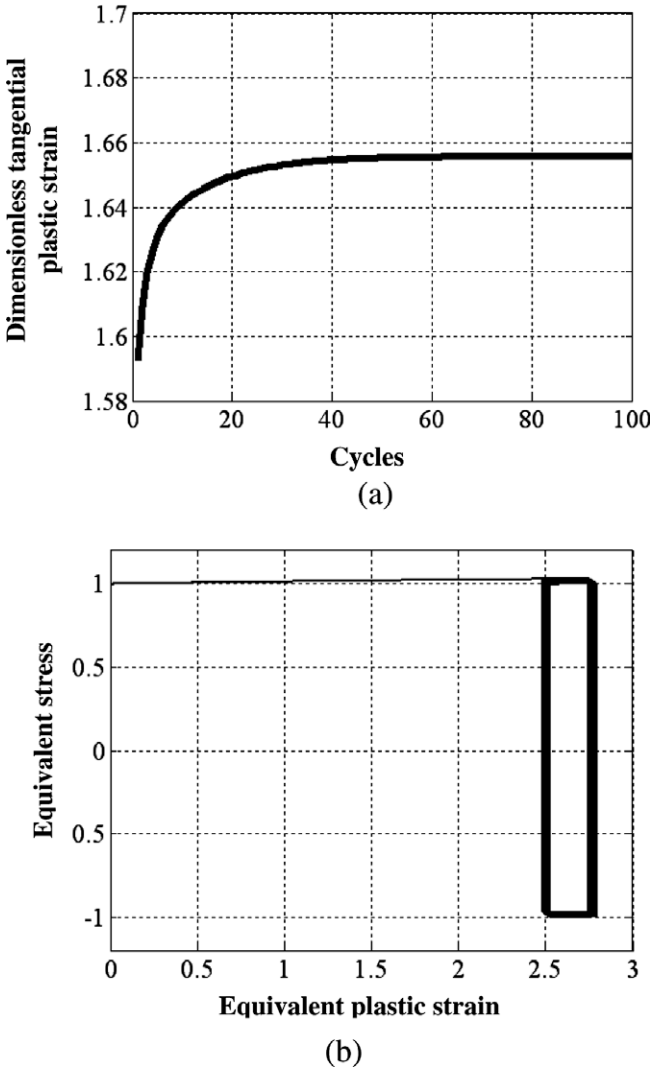

Fig. 5. Plastic shakedown behavior of the thin cylinder for $\tau_{max} = 2.196$ and $\sigma_p = 0.5$, material models constants and thin cylinder geometry are given in Table 1. (a) Variation of the maximum nondimensional tangential plastic strain, e_θ^p at the outer surface of the thin cylinder as a function of the number of thermal loading cycles and (b) normalized equivalent stress versus normalized equivalent plastic strain at the outer surface.

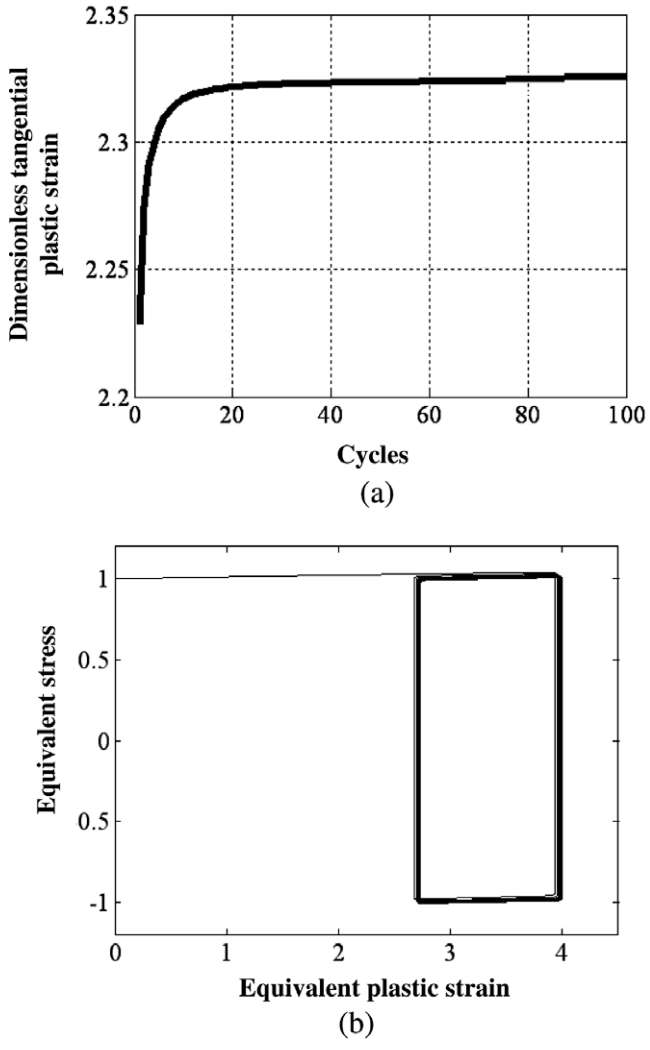

Fig. 6. Ratcheting behavior of the thin cylinder for $\tau_{max} = 2.928$ and $\sigma_p = 0.5$, material models constants and thin cylinder geometry are given in Table 1. (a) Variation of the maximum nondimensional tangential plastic strain, e_θ^p, at the outer surface of the thin cylinder as a function of the number of thermal loading cycles and (b) normalized equivalent stress versus normalized equivalent plastic strain at the outer surface.

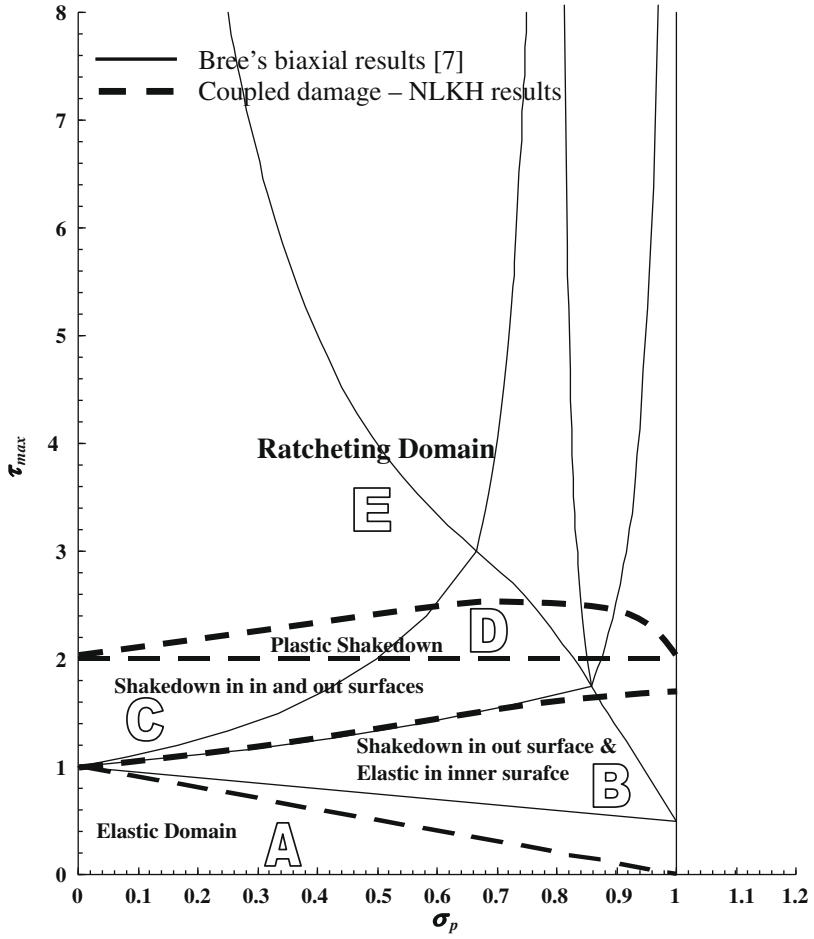

Fig. 7. Interaction diagram for thermal load parameter, τ_{max}, versus internal pressure loading parameter, σ_p, solid line (—) shows the two-dimensional Bree's diagram and the dashed line () presents the new results based on the continuum damage mechanics.

$$S_\theta^{Trial,n+1} = (1-\varpi_n)\left(\frac{\sigma_p + \frac{1}{(1-\upsilon^2)}\left[\int_{\frac{-1}{2}}^{\frac{1}{2}}(1-\varpi_n)(e_\theta^{p,n}+\upsilon e_z^{p,n}+\tau_n)d\eta\right]}{\int_{\frac{-1}{2}}^{\frac{1}{2}}(1-\varpi_n)d\eta} - \frac{1}{(1-\upsilon^2)}(e_\theta^{p,n}+\upsilon e_z^{p,n}) - \tau_n\right) + \frac{(1-\varpi_n)}{\int_{\frac{-1}{2}}^{\frac{1}{2}}(1-\varpi_n)d\eta}\int_{\frac{-1}{2}}^{\frac{1}{2}}(1-\varpi_n)\Delta\tau d\eta - (1-\varpi_n)\Delta\tau \quad (36)$$

$$S_z^{Trial,n+1} = (1-\varpi_n)\left(\frac{\sigma_p + \frac{1}{(1-\upsilon^2)}\left[\int_{\frac{-1}{2}}^{\frac{1}{2}}(1-\varpi_n)(e_z^{p,n}+\upsilon e_\theta^{p,n}+\tau_n)d\eta\right]}{\int_{\frac{-1}{2}}^{\frac{1}{2}}(1-\varpi_n)d\eta} - \frac{1}{(1-\upsilon^2)}(e_z^{p,n}+\upsilon e_\theta^{p,n}) - \tau_n\right) + \frac{(1-\varpi_n)}{\int_{\frac{-1}{2}}^{\frac{1}{2}}(1-\varpi_n)d\eta}\int_{\frac{-1}{2}}^{\frac{1}{2}}(1-\varpi_n)\Delta\tau d\eta - (1-\varpi_n)\Delta\tau \quad (37)$$

$\Delta\tau$ is the increment of nondimensional temperature difference across the thickness. It is assumed that the maximum pressure is not greater than the yield pressure and elastic solution is only needed for pressure loading. The loading associated with the thermal gradient is cyclic and can be considered with the constant pressure loading. With these trial stresses, the yield function (Eq. (33)) is verified. If the yield criterion is violated, plastic solution is used. With the help of the incremental form of Eqs. (14), (15), (30), (31), and (34) as below and using Newton–Raphson method for Eq. (33), the plastic strains increment can be determined

$$\varepsilon_{n+1} = \varepsilon_{n+1}^{Trial} + \Delta\varepsilon_{n+1}^p \quad (38)$$

$$\varepsilon_{n+1}^p = \varepsilon_n^p + \Delta\varepsilon_{n+1}^p \quad (39)$$

$$X_{n+1} = X_n + (1-\varpi_{n+1})\left(\frac{2}{3}C\Delta\varepsilon_{n+1}^p - \gamma X_{n+1}\Delta p_{n+1}\right) \quad (40)$$

$$\varpi_{n+1} = \varpi_n + \left(\frac{Y_{n+1}}{S}\right)^s \Delta p_{n+1} \quad (41)$$

$$\Delta p_{n+1} = \frac{2}{\sqrt{3}}\left(\left(\Delta\varepsilon_z^{p,n+1}\right)^2 + \left(\Delta\varepsilon_\theta^{p,n+1}\right)^2 + \Delta\varepsilon_z^{p,n+1}\Delta\varepsilon_\theta^{p,n+1}\right)^{\frac{1}{2}} \quad (42)$$

$$\frac{\Delta\varepsilon_z^{p,n+1}}{\Delta\varepsilon_\theta^{p,n+1}} = \frac{2\tilde{\sigma}_z^{n+1} - \tilde{\sigma}_\theta^{n+1} - 2X_z + X_\theta}{2\tilde{\sigma}_\theta^{n+1} - \tilde{\sigma}_z^{n+1} - 2X_\theta + X_z} \quad (43)$$

Table 2
Material models constants and applied loadings.

	γ	Q (MPa)	q	τ_{max}	σ_p	Fig.
I	250	0.06	2	2.928	0.5	8a
II	250	0.6	0.5	2.928	0.5	8b
III	250	0.06	2	2.196	0.5	8c
IV	250	0.6	0.5	2.196	0.5	8d
V	50	0.6	2	2.196	0.5	9a
VI	50	0.6	2	2.928	0.5	9b

$$S_\theta^{n+1} = (1-\varpi_{n+1})\left(\frac{\sigma_p + \frac{1}{(1-\upsilon^2)}\left[\int_{\frac{-1}{2}}^{\frac{1}{2}}(1-\varpi_{n+1})\left(e_\theta^{p,n+1}+\upsilon e_z^{p,n+1}+\tau_{n+1}\right)d\eta\right]}{\int_{\frac{-1}{2}}^{\frac{1}{2}}(1-\varpi_{n+1})d\eta} - \frac{1}{(1-\upsilon^2)}\left(e_\theta^{p,n+1}+\upsilon e_z^{p,n+1}\right)-\tau_{n+1}\right) \quad (44)$$

$$S_z^{n+1} = (1-\varpi_{n+1})\left(\frac{\sigma_p + \frac{1}{(1-\upsilon^2)}\left[\int_{\frac{-1}{2}}^{\frac{1}{2}}(1-\varpi_{n+1})\left(e_z^{p,n+1}+\upsilon e_\theta^{p,n+1}+\tau_{n+1}\right)d\eta\right]}{\int_{\frac{-1}{2}}^{\frac{1}{2}}(1-\varpi_{n+1})d\eta} - \frac{1}{(1-\upsilon^2)}\left(e_z^{p,n+1}+\upsilon e_\theta^{p,n+1}\right)-\tau_{n+1}\right) \quad (45)$$

5. Results and discussion

The constitutive model parameters for $2\frac{1}{4}$ CrMo steel at 580 °C were given by Lemaitre and Desmorat [16] and are shown in Table 1. Model constants are temperature dependent but the average values were chosen and it was assumed that the mean temperature is constant during loading and unloading. The mean radius, R, and thickness, t, are 100 mm and 10 mm, respectively.

Constant mechanical and cyclic thermal loading were applied. Maximum inside pressure (mechanical loading) was not allowed to exceed the yield pressure. Starting from zero, an incremental thermal loading with a linearly varying temperature difference distribution across the wall thickness was applied. When the linear temperature gradient attained its maximum, it was reduced incrementally to zero. At this point, a full thermal stress cycle is completed. The number of loading increments varies in different load cases in the test matrix, as each increment applies less than 1 °C in temperature gradient. Up to 100 load increments per cycle and up to 1000 cycles are applied in the most severe temperature gradients. In some cases, a steady cyclic state stress–strain plot is attained after the first cycle.

As an example, the amplitude of the nondimensional cyclic thermal gradient across the thin wall of the cylinder, τ_{max}, and the nondimensional constant mechanical stress, σ_p, were assumed to be 1.976 and 0.5, respectively. Fig. 4a shows the variation of the tangential plastic strain at the outer surface of the thin cylinder as a function of the number of cycles. Plastic strain stays constant during cyclic loading. Fig. 4b shows the variation of the equivalent stress as a function of equivalent plastic strain at the outer surface. The thin cylinder behavior is elastic after the first cycle and elastic shakedown was obtained in the first cycle. The amplitude of the nondimensional temperature gradient was increased to $\tau_{max} = 2.196$ and nondimensional mechanical stress was not changed ($\sigma_p = 0.5$). Plastic shakedown was obtained (Fig. 5a and b). Fig. 5a shows that the nondimensional tangential plastic strain at the outer surface stays constant after 62nd cycle and the equivalent stress-equivalent plastic strain loop does not evolve (Fig. 5b). Finally, as it was shown in Fig. 6a, when the cyclic and constant loadings are $\tau_{max} = 2.928$ and $\sigma_p = 0.5$, respectively, the plastic strain at the outer surface increases with a constant slope in each loading cycle. Fig. 6b shows that the stress–strain loop evolves and ratcheting phenomenon was resulted.

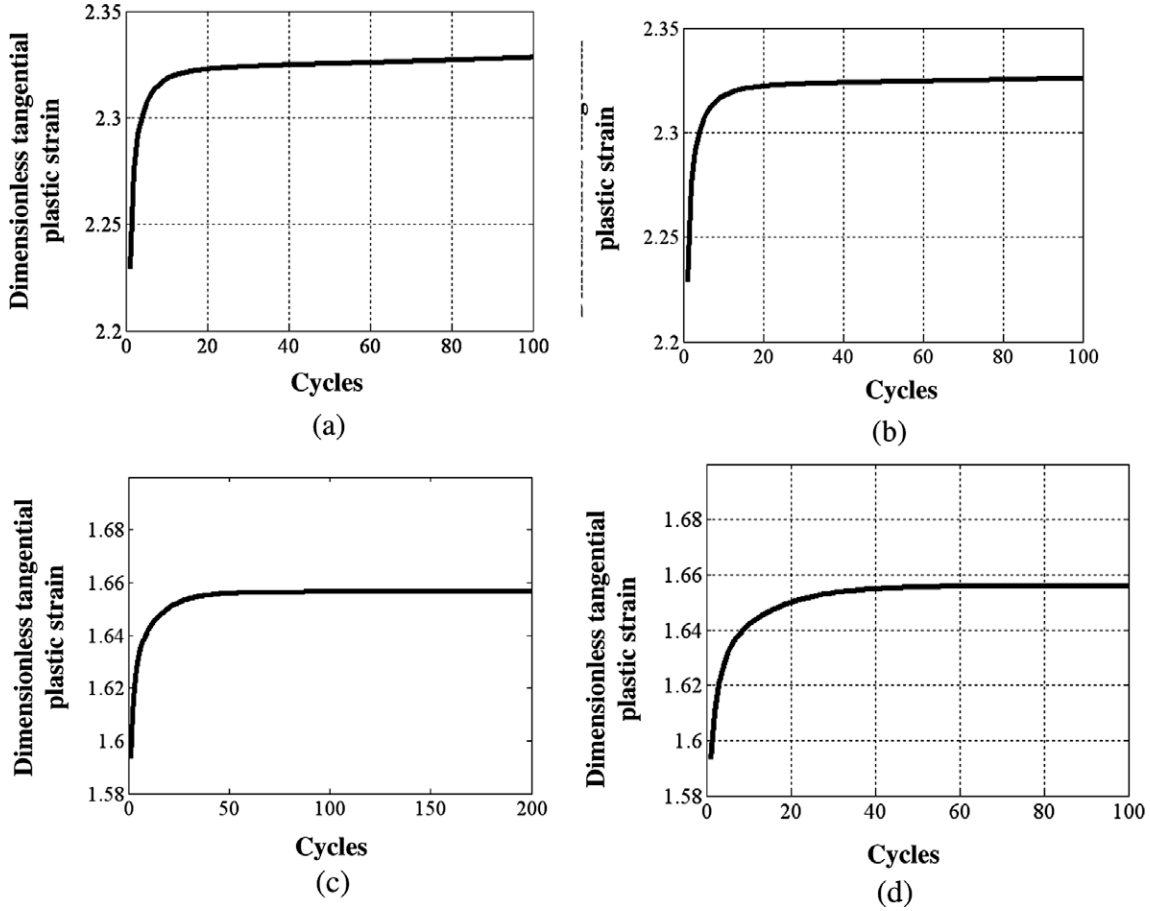

Fig. 8. Variation of the maximum nondimensional tangential plastic strain, e_θ^p at the outer surface as a function of the number of thermal loading cycles for $\tau_{max} = 2.928$ and $\sigma_p = 0.5$: (a) $Q = 0.06$ MPa (Table 2, case I), (b) $q = 0.5$ (Table 2, case II), and $\tau_{max} = 2.196$ and $\sigma_p = 0.5$: (c) $Q = 0.06$ MPa (Table 2, case III) and (d) $q = 0.5$ (Table 2, case IV) (for each case, other material constants are given in Table 1).

Different results were obtained for the inner and outer surfaces of the thin cylinder, with changing the applied mechanical and thermal loading. In order to identify different regions in the Bree's diagram, more than 100 combinations of mechanical and thermal loadings were simulated. The Bree's diagram is divided into different regions as a function of the first yield situation and the inner and outer surface of the thin cylinder behavior. These regions are shown in Fig. 7 which is known as the Bree's diagram. In order to obtain the interaction diagram for Bree's results [7], the inner pressure and the temperature gradient were normalized according to Eqs. (32).

It should be noted that the Bree's model was obtained using the Tresca's criterion. In the present study, the von-Mises criterion was used. In order to be able to compare the results, the inner pressure in this study was normalized using the following relation: $\sigma_p = \frac{\sqrt{3}}{2}\frac{Pr}{t\sigma_y}$.

Region A in Fig. 7 corresponds to the elastic answer. The outer surface of the thin cylinder yields and elastic shakedown begins with increasing the temperature difference (region B). The inner surface remains elastic. In the third region C, the inner surface also yields and both surfaces are in elastic shakedown. When maximum thermal stress reaches $2\sigma_y$, the plastic strain loops are formed and plastic shakedown is obtained (region D). For the thermal and mechanical stresses in the region D, the inner and outer surfaces have the same behavior and both are in plastic shakedown state. Finally, the ratcheting was obtained for two directions in the thin walled cylinder, in the region E. Continuum damage mechanics, which is dependent on the accumulated plastic strain, limits the plastic shakedown zone. The new boundaries were obtained by applying constant internal pressure while the temperature gradient was increased gradually to obtain each boundary between elastic, elastic shakedown, plastic shakedown, and ratcheting.

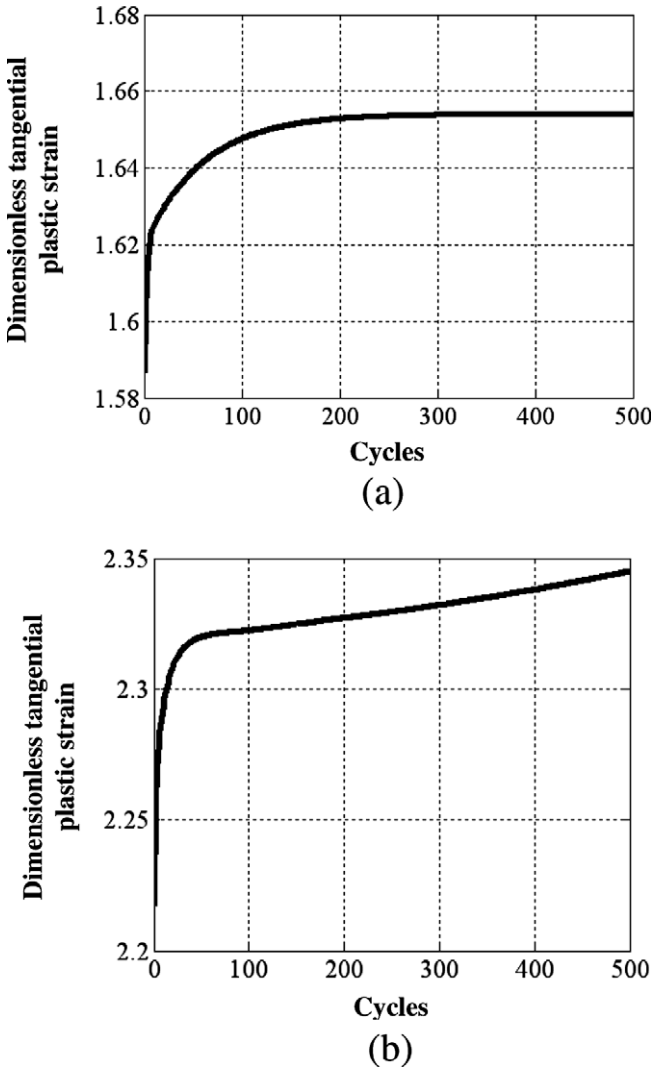

Fig. 9. Variation of the maximum nondimensional tangential plastic strain, e_θ^p at the outer surface as a function of the thermal loading cycles when nonlinear kinematic hardening constant, γ, was decreased to 50 and the loadings are (a) $\tau_{max} = 2.196$ and $\sigma_p = 0.5$ (Table 2, case V), (b) $\tau_{max} = 2.928$ and $\sigma_p = 0.5$ (Table 2, case VI) (for each case, other material constants are given in Table 1).

As it was shown in the Bree's diagram (Fig. 7), the two dimensional model of Bree can not predict the ratcheting because of the damage progress due to the accumulated plastic strain. But the $2\sigma_y$ limit of the shakedown behavior is independent of the models and the material behavior. Taking into consideration the nonlinear kinematic hardening behavior into the model, leads to the shift of the boundary between the plastic shakedown and ratcheting for greater internal pressures.

It should be noted that other simulations have been conducted using different values of the damage model constants, Q and q. Although, the rate of ratcheting and the number of cycles before shakedown were changed, the same boundaries between different material behaviors were obtained. In the following simulations, one of the parameters, Q, q and γ were changed in each example, and other material models parameters were as the same values in Table 1. Table 2 gives the used material models constants in these simulations and Figs. 8 and 9 show the variation of the nondimensional plastic strain as a function of the number of thermal loading cycles. For the fist simulation, material damage model constant, Q, was decreased to 0.06 with respect to the simulations of Fig. 7. The cyclic thermal and constant mechanical loadings are $\tau_{max} = 2.928$ and $\sigma_p = 0.5$, respectively (case I, Table 2). For the same loading, ratcheting behavior had been resulted for $Q = 0.6$ (see Fig. 6) and the same behavior was obtained for $Q = 0.06$ (Fig. 8a). In order to show the effect of the other material damage constant, q, on the thin cylinder behavior, the loadings were not changed and q was decreased to 0.5 (case II, Table 2). For this case, Fig. 8b shows that the behavior of the thin cylinder under theses loadings was not changed.

Two other examples were considered for shakedown behavior. The loadings were changed to $\tau_{max} = 2.196$ and $\sigma_p = 0.5$, and Q parameter was set to 0.06 (case III, Table 2). For the next simulation, the loadings were not changed and q parameter was diminished to 0.5 (case IV, Table 2). In both cases, plastic shakedown behavior was obtained (Fig. 8c and d). It was shown in Fig. 5 that the behavior was also plastic shakedown for the same loadings.

The effect of the, γ, constant of the kinematic hardening model was studied with changing it to 50. For two different above loadings (case V and VI, Table 2), the behavior of the thin cylinder was unchanged. As it was shown in Fig. 9a, number of cycles needed for plastic shakedown, was increased from 62 (Fig. 5a) to 300, and the rate of ratcheting was increased (Fig. 9b).

6. Conclusions

The results of Kang et al. [15] showed that the coupling continuum damage mechanics and cyclic constitutive models, can improve the prediction of materials behavior in cyclic loading. Motivated by their results, the behavior of the Bree's cylinder was studied with combining the unified continuum damage law and the nonlinear kinematic hardening model. The behavior of thin cylinder subjected to the constant internal pressure and the cyclic temperature gradient was studied. The effect of damage was considerable and the plastic shakedown domain obtained for low pri-

mary stresses and cyclic temperature by Bree [7] was modified. Taking into consideration the hardening effect, which was neglected in Bree's analysis, shifts the plastic shakedown boundary for higher internal pressure. The role of the material constants was also studied. It was shown that the variation of these constants did not change the behavior of materials, however, the rate of the accumulated plastic strain and cycles needed to obtain plastic shakedown were affected. It should be noted that because of the creep strains, the continuum damage mechanics of the creep mechanisms must also be considered in order to obtain more realistic boundaries in the interaction diagram. This will be the subject of a future research.

Acknowledgments

Discussions and advice of Professor M. Mahzoon (Shiraz University) and Dr. M. Dadfarnia (University of Illinois at Urbana Champaign) are appreciated.

References

[1] Hassan T, Lakhdar T, Krishna S. Influence of non-proportional loading on ratcheting responses and simulations by two recent cyclic plasticity models. Int J Plast 2008;24:1863–89.
[2] Abdel-Karim M. Shakedown of complex structures according to various hardening rules. Int J Pressure Vess Piping 2005;82:427–58.
[3] Parkes EW. Structural effects of repeated thermal loading. In: Benham et al., editors. Thermal stress. London: Pitman; 1964.
[4] Miller PR. Thermal stress ratchet mechanism in pressure vessels. J Basic Eng, Trans ASME, Ser D 1959;81:190–6.
[5] Jiang W, Leckie FA. A direct method for the shakedown analysis of structures under sustained and cyclic loads. ASME J Appl Mech 1992;59:251–60.
[6] Bree J. Elastic–plastic behaviour of thin tubes subjected to internal pressure and intermittent high heat fluxes with application to fast nuclear reactor fuel elements. J Strain Anal 1967;2:226–38.
[7] Bree J. Plastic deformation of a closed tube due to interaction of pressure stresses and cyclic thermal stresses. Int J Mech Sci 1989;31:865–92.
[8] ASME boiler and pressure vessel code. Section III division I subsection NH, Appendix T. New York: American Society of Mechanical Engineering; 2003.
[9] Mulcahy TM. Thermal ratcheting of a beam element having an idealized Bauschinger effect. ASME J Eng Mater Technol 1976;98:264–71.
[10] Chinh PD. Shakedown theory for elastic plastic kinematic hardening bodies. Int J Plast 2007;23:1240–59.
[11] Abdalla HF, Megahed MM, Younan YA. Determination of shakedown limit load for a 90-degree pipe bend using a simplified technique. ASME J Pressure Vess Technol 2006;128:618–24.
[12] Hachemi A, Weichert D. Numerical shakedown analysis of damaged structures. Comput Methods Appl Mech Eng 1998;160:57–70.
[13] Druyanov B, Roman I. On adaptation (shakedown) of a class of damaged elastic plastic bodies to cyclic loading. Eur J Mech A/Solids 1997;17:71–8.
[14] Nayebi A, El Abdi R. Shakedown analysis of beams using nonlinear kinematic hardening materials coupled with continuum damage mechanics. Int J Mech Sci 2008;50:1247–54.
[15] Kang G, Liu Y, Gao Q. Uniaxial ratcheting and fatigue failure of tempered 42CrMo steel: damage evolution and damage-coupled visco-plastic constitutive model. Int J Plast 2008;25:838–60.
[16] Lemaitre J, Desmorat R. Engineering damage mechanics. Berlin: Springer-Verlag; 2005.
[17] Sehitoglu H, Gall K, Garcia AM. Recent advances in fatigue crack growth modeling. Int J Fract 1996;80:165–92.
[18] Bari S, Hassan T. Anatomy of coupled constitutive models for ratcheting simulation. Int J Plast 2000;16:381–409.
[19] Hassan T, Taleb L, Krishna S. Influence of non-proportional loading on ratcheting responses and simulations by two recent cyclic plasticity models. Int J Plast 2008;24:1863–89.
[20] Rahman SM, Hassan T, Corona E. Evaluation of cyclic plasticity models in ratcheting simulation of straight pipes under cyclic bending and steady internal pressure. Int J Plast 2008;24:1756–91.
[21] Colak OU. Kinematic hardening rules for modelling uniaxial and multiaxial ratcheting. Material Des 2008;29:1575–81.
[22] Armstrong PJ, Frederick CO. A mathematical representation of the multi-axial Bauschinger effect. CEGB report no. RD/B/N 731; 1966.
[23] Kumar P, Nukala VV. A return mapping algorithm for cyclic viscoplastic constitutive models. Comput Methods Appl Eng 2006;195:148–78.
[24] Hopperstad OS, Remseth S. A return mapping algorithm for a class of cyclic plasticity models. Int J Numer Methods Eng 1995;38:549–64.